

Supporting Information

Structural characterization of agonist binding to protease-activated receptor 2 through mutagenesis and computational modeling

Amanda J Kennedy,^{†,⊥} Flavio Ballante,^{§,⊥} Johan R Johansson,[‡] Graeme Milligan,^{||} Linda
Sundström,^{*,†} Anneli Nordqvist[‡], and Jens Carlsson^{*,§}

[†]Discovery Sciences and [‡]Cardiovascular Renal and Metabolism, IMED Biotech Unit,
AstraZeneca, Gothenburg, SE-431 83 Mölndal, Sweden

[§]Science for Life Laboratory, Department of Cell and Molecular Biology, Uppsala University,
BMC Box 596, SE-751 24 Uppsala, Sweden

^{||}Centre for Translational Pharmacology, Institute of Molecular, Cell and Systems Biology,
College of Medical, Veterinary and Life Sciences, University of Glasgow, Glasgow G12 8QQ,
United Kingdom

[⊥]These authors contributed equally to this work.

* Corresponding authors: linda.sundstrom@astrazeneca.com; jens.carlsson.lab@icm.uu.se

Number of pages: 20

Number of Figures: 13

Number of Tables: 3

Table of Contents

Western Blot method	S3
Competition Binding method	S3
Figures	S4
Tables	S16
References	S20

METHODS

Western blot. Parental 1321N1 and PAR2 transiently-transfected cells were seeded at 200000 cells/well in a 6 well plate and incubated overnight at 37 °C, 5% CO₂. The cells were detached, washed with PBS and the pellet was resuspended in 200 µl PBS. These lysates were then frozen at -20 °C before use. Samples (40 µL) were prepared for western blot using 4× NuPAGE samples buffer and 10× NuPAGE reducing buffer and heated at 70 °C for 10 min. These were loaded (10 µL) onto a NuPAGE 4-12% Bis-Tris 17-well, 1.0 mm gel and run at constant 200 V for 35 min in MES running buffer. The proteins were then transferred onto a 0.2 µm PVDF membrane using the Trans-Blot Turbo Transfer system according to the manufacturer's instructions. The membrane was then blocked with PBS containing 5% BSA, incubated with anti-PAR2 (D61D5, Cell Signaling Technology) and visualized using an anti-Rabbit AP conjugate and 1-step NBT/BCIP substrate solution (ThermoFisher).

Competition Binding. Competition binding experiments with selected modified peptides against radiolabeled [³H]-GB110 were carried out on membranes isolated from HEKexp293F cells expressing human PAR2. In 96-well plates, at final assay concentration stated in parentheses, protein (30 µg/well), label (25 nM), and competing peptides (35 pM – 1 mM) or unlabeled GB110 (0.3 nM – 10 µM) were incubated for 2 h at room temperature with shaking. The reaction was then filtered through 0.5% PEI coated filter plates using a BiomekFX. The filterplate was then dried for 1 h at 50 °C. Scintillation fluid was then added to each well, before reading the plate in a Microbeta reader. Data were analyzed to obtain the pK_i (-log₁₀ dissociation constant) of competing ligands determined by the Cheng and Prusoff equation using the IC₅₀ values (concentration of inhibitor, in this case unlabeled SLIGKV and modified peptides, that reduces the response by 50%) derived from competitions curves using GraphPad Prism 7.¹

FIGURES

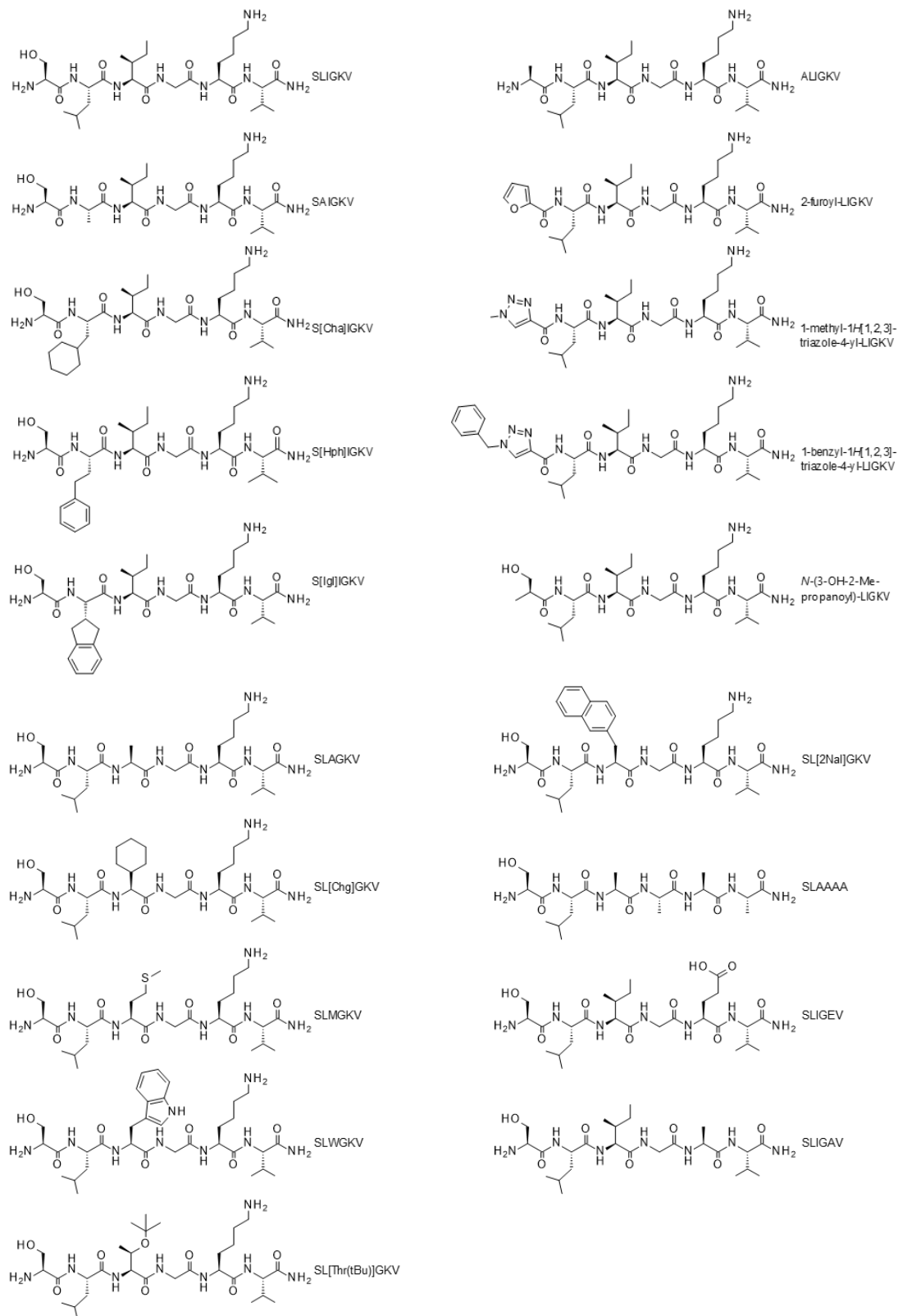


Figure S1. 2D structures of peptides included in this study.

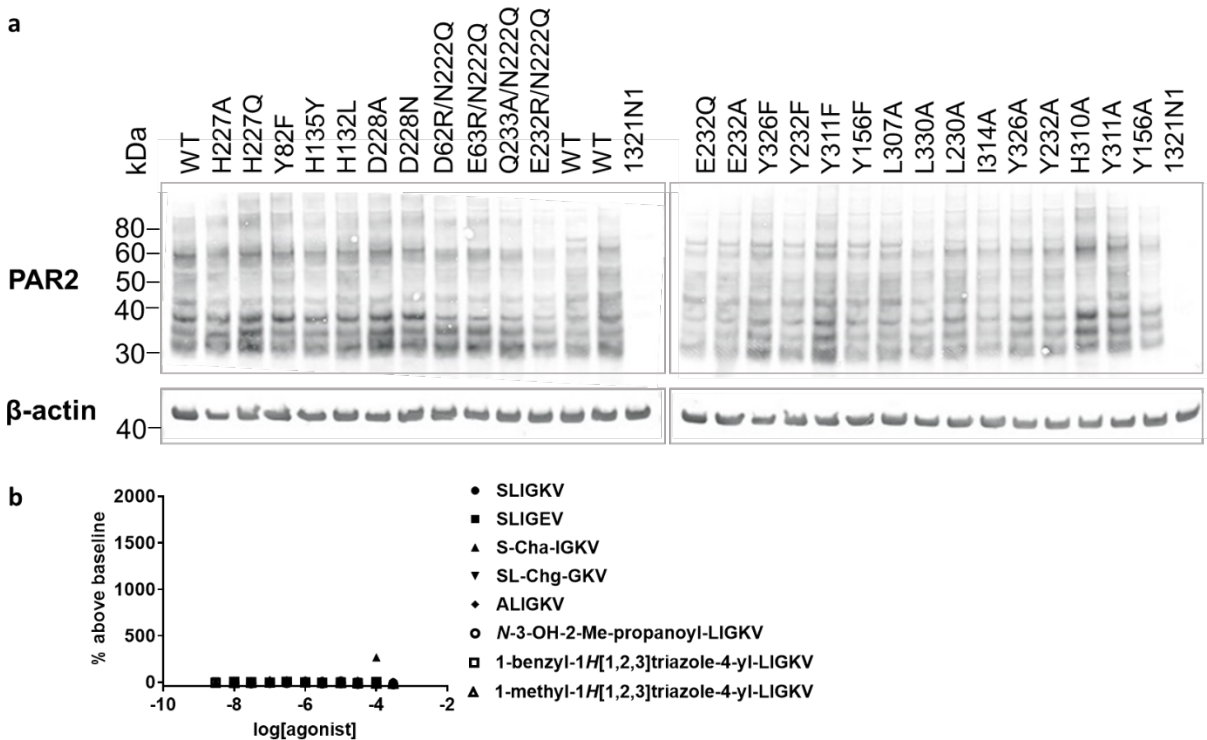


Figure S2. Control data. (a) Western blot analysis of transiently-transfected mutant and WT PAR2 showing receptor expression, and (b) representative selection of all agonists included in this study that gave no calcium mobilization response in 1321N1 parental cell line. Data are presented as mean±s.e.m of n=3 independent experiments.

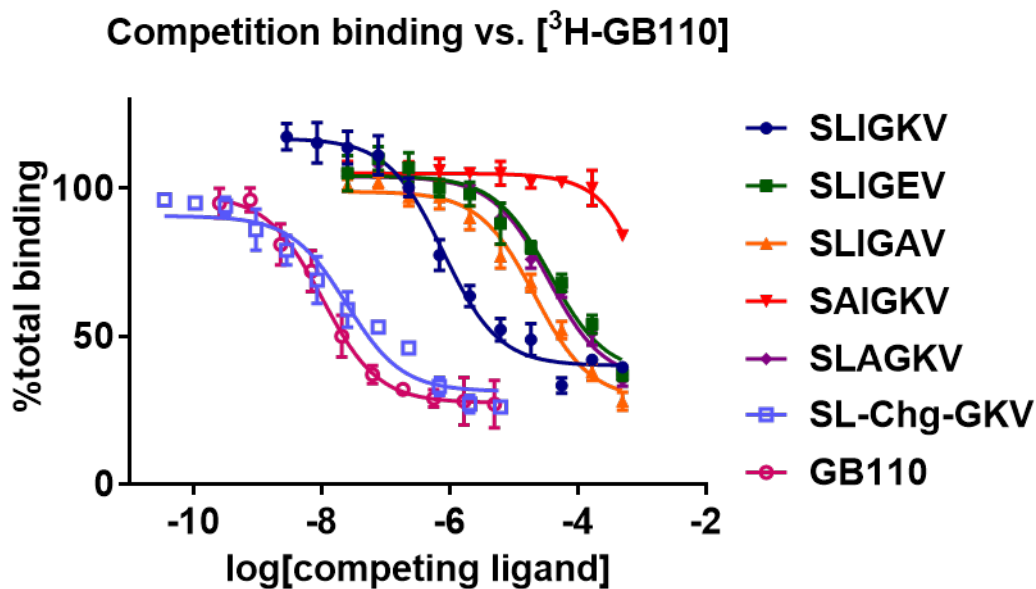


Figure S3. Binding data of selected mutant SLIGKV peptides. Data, from radioligand competition binding assays, are presented as mean±s.e.m of n=2-3 independent experiments.

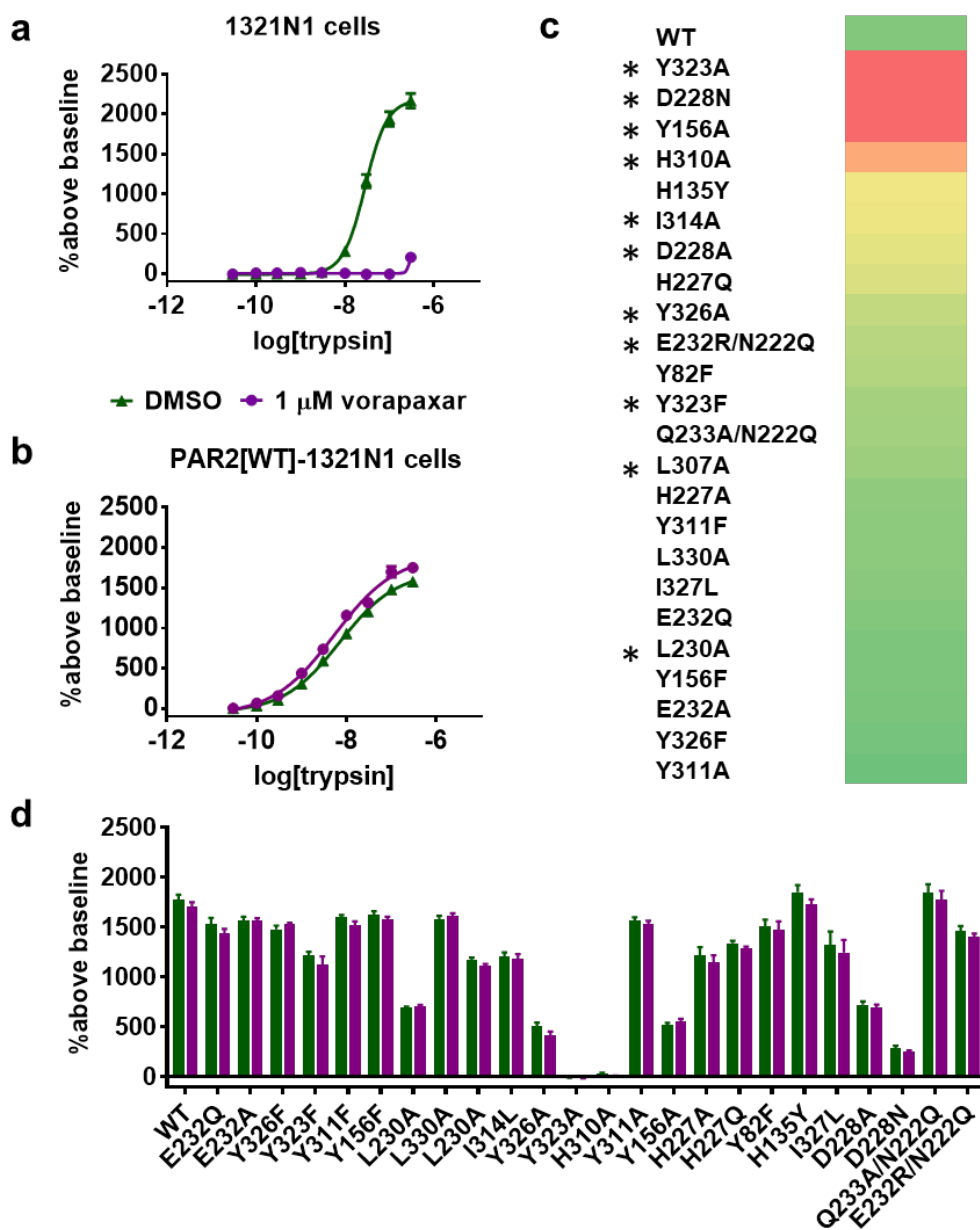


Figure S4. Trypsin-induced activation of PAR2 mutants. (a) Trypsin activated calcium signaling in the 1321N1 parental cell line (green) and this response was blocked by addition of PAR1 antagonist vorapaxar (1 μ M, purple). (b) Trypsin-induced activation of WT PAR2 was unaffected by addition of vorapaxar. (c) Heat plot of fold change of trypsin-induced activation of calcium mobilization at mutant PAR2 receptors presented on a color scale where red and green correspond to >10 -fold drop in potency and similar effect as WT, respectively. Asterisks highlight the residues identified as important in SLIGKV-induced activation of PAR2. (d) Response of SLIGKV (10 μ M) in the presence (purple) and absence (green) of vorapaxar, suggesting that vorapaxar does not interact with the PAR2 mutants. Activation of PAR2 was monitored using a calcium mobilization assay. Data are presented as mean \pm s.e.m of n=3 independent experiments.

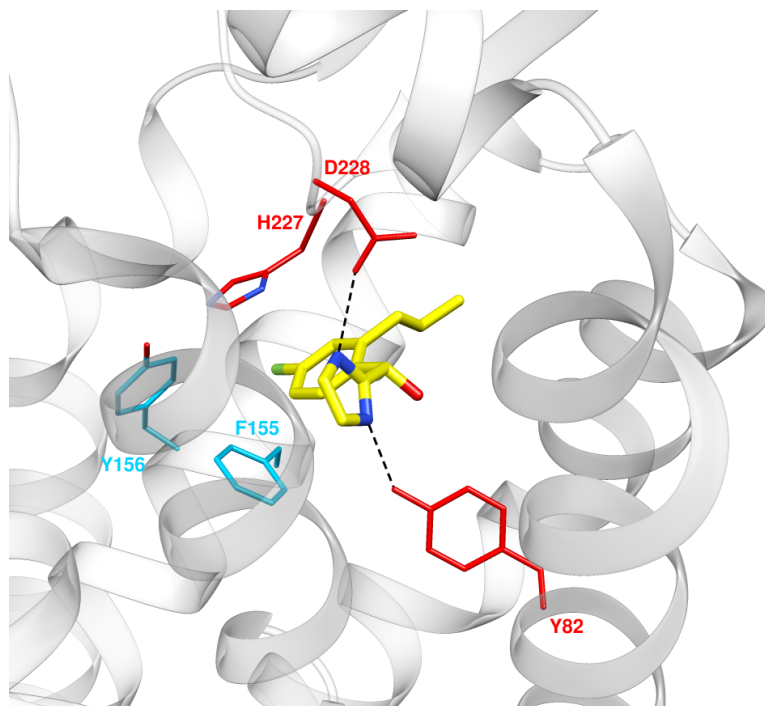


Figure S5. Crystal structure of PAR2 in complex with AZ8838 (PDB code 5NDD).² AZ8838 and selected residues are shown in sticks. Hydrogen bonds with Y82^{1,39} and D228^{ECL2} are represented as dashed lines. Receptor residues have been color-coordinated based on their spatial arrangement.

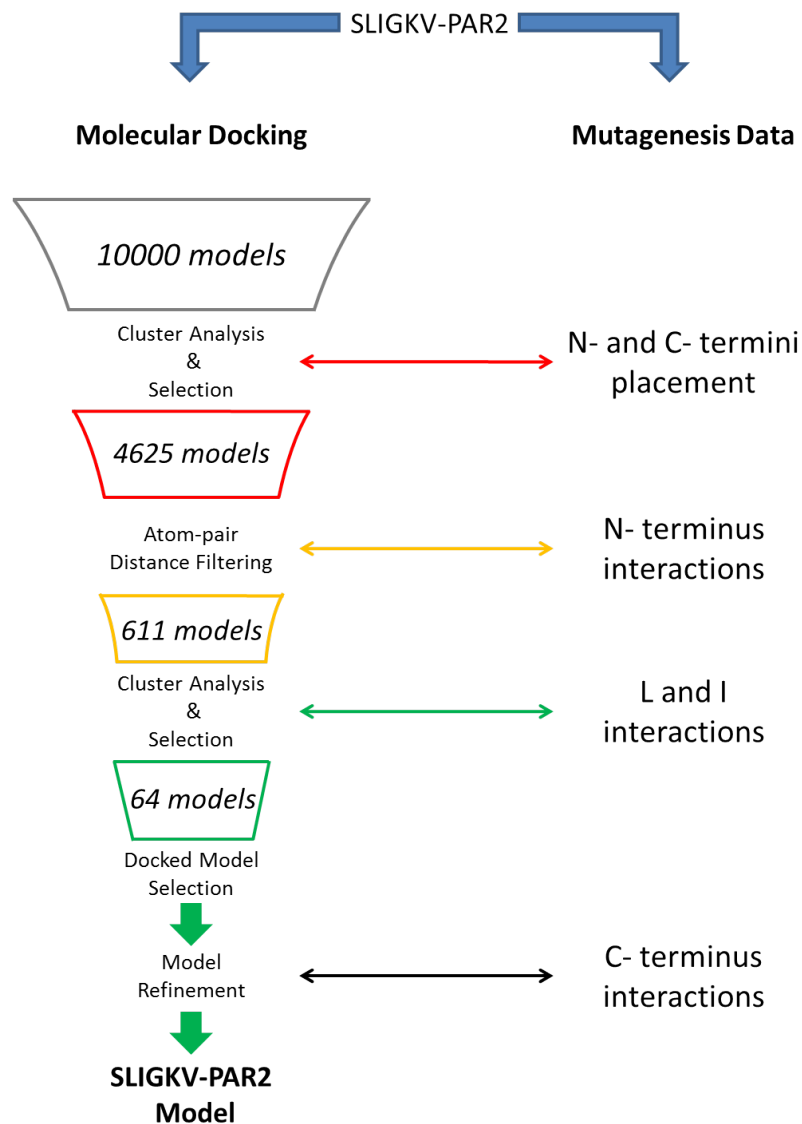


Figure S6. Mutagenesis-driven structure-based modeling of the PAR2-SLIGKV complex. Molecular docking generated an initial ensemble of 10000 models of SLIGKV in the PAR2 crystal structure. The final model was obtained by: (1) Selection of a cluster of models (a total of 4625) showing a spatial placement of the N- and C-termini in agreement with the experimental data; (2) Filtering of the previously selected set of models according to the N-terminus interactions. 611 models passed this filter; (3) Re-clustering of the remaining models based on the leucine and isoleucine of SLIGKV. A cluster with 64 structures was then selected and a representative complex was refined to obtain the final model.

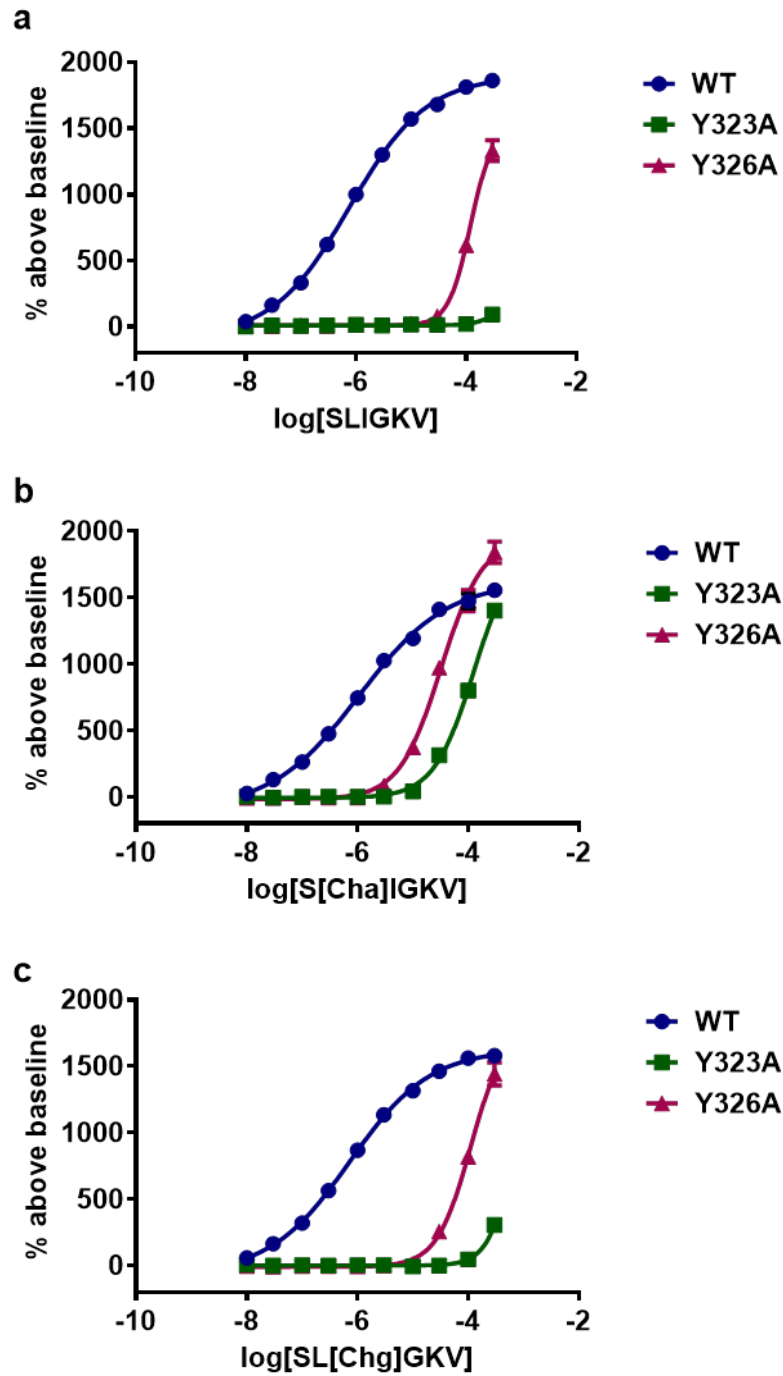


Figure S7. Concentration-response curves of (a) SLIGKV, (b) S[Cha]IGKV and (c) SL[Chg]GKV at WT PAR2 and selected mutant receptors. Receptor activation was measured using a calcium mobilization assay and data are expressed as mean±s.e.m of n=3 independent experiments.

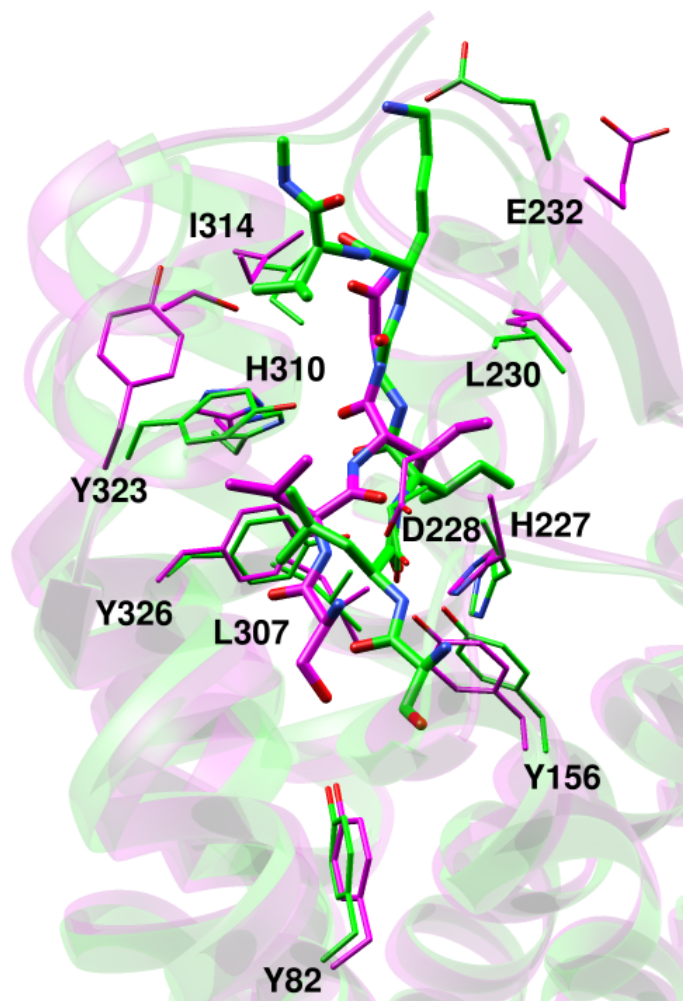


Figure S8. Overlay of SLIG (magenta) and SLIGKV (green) complexes obtained from ligand-centric and molecular docking protocols, respectively. The ligands and selected residues are shown in sticks.

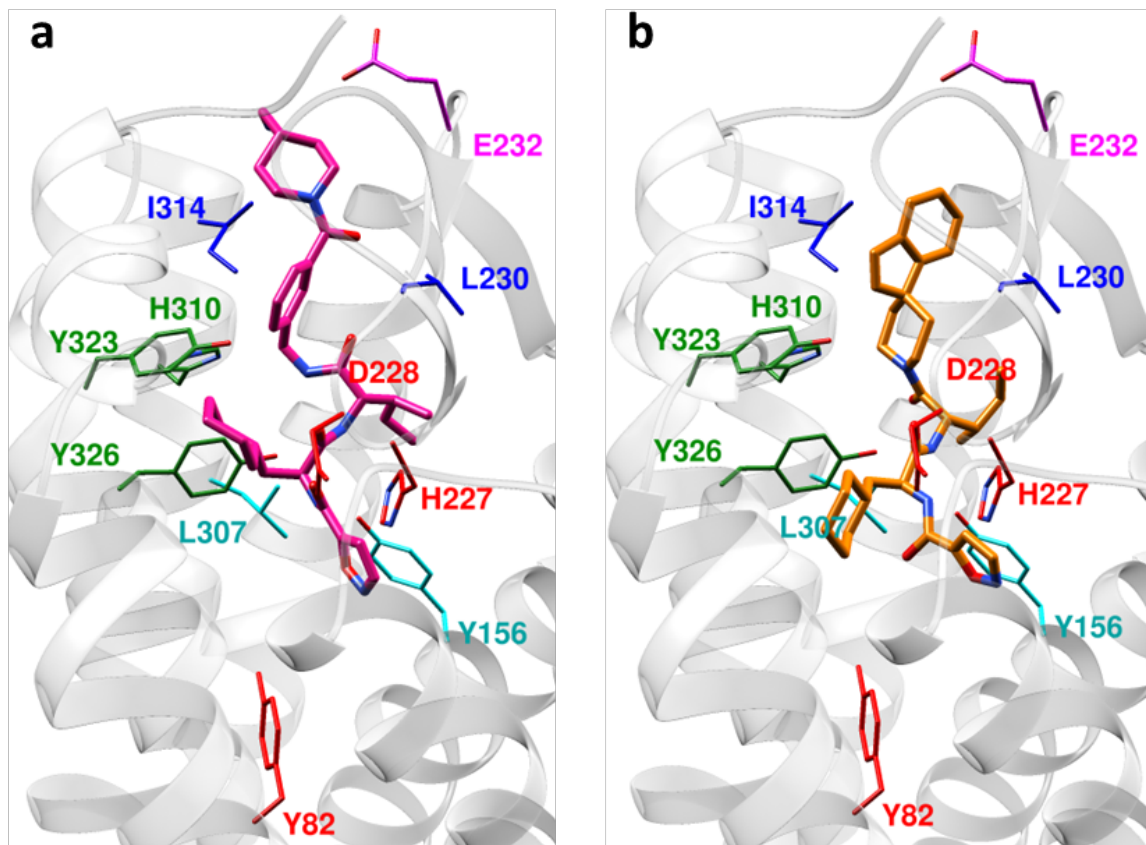


Figure S9. Predicted binding modes of (a) GB110 and (b) GB88. The ligands and selected residues are shown in sticks. The complexes were obtained by molecular docking to the model of agonist-bound PAR2. Receptor residues have been color-coordinated based on their spatial arrangement.

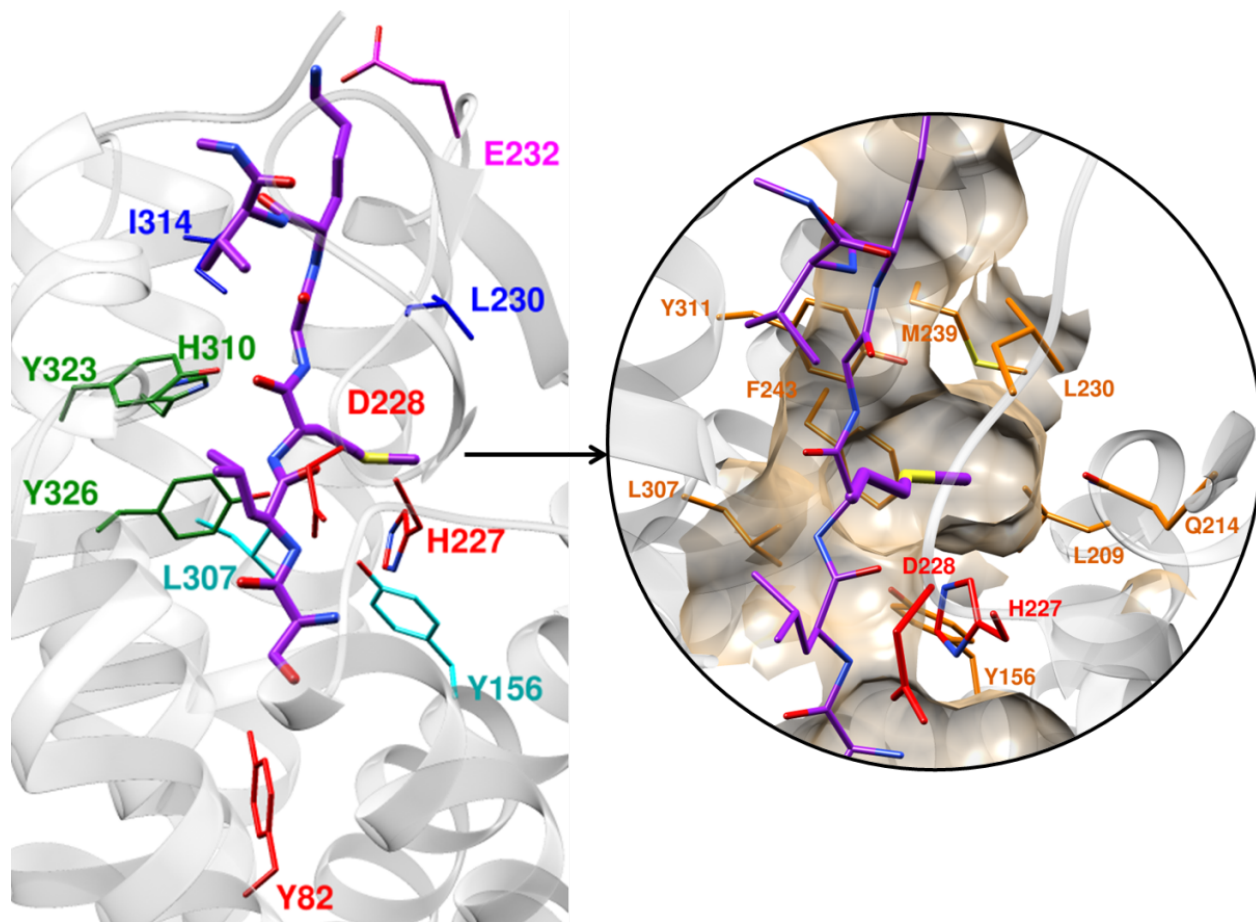


Figure S10. Predicted binding mode of SLMGKV. The ligand and selected residues are shown in sticks. The complex was obtained by molecular docking to the model of agonist-bound PAR2. Receptor residues have been color-coordinated based on their spatial arrangement.

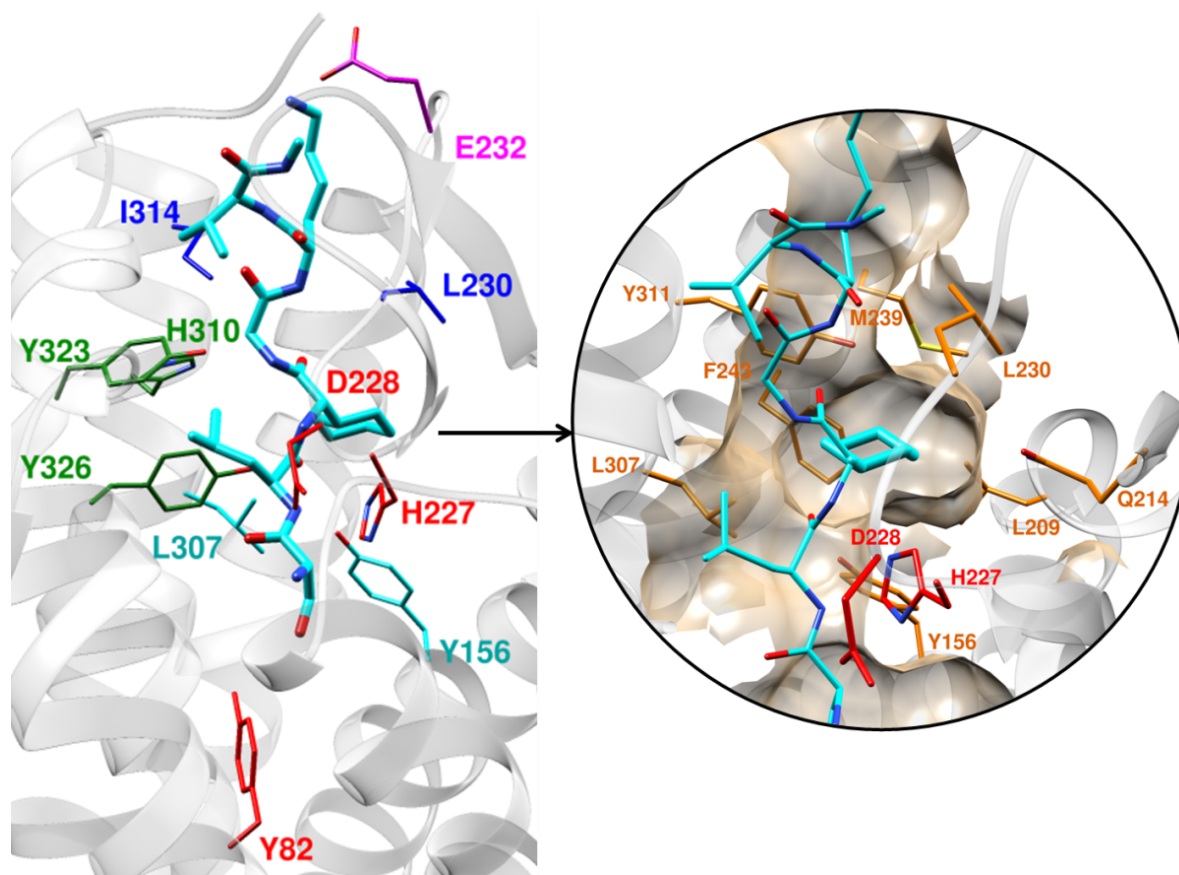


Figure S11. Predicted binding mode of SL[Chg]GKV. The ligand and selected residues are shown in sticks. The complex was obtained by molecular docking to the model of agonist-bound PAR2. Receptor residues have been color-coordinated based on their spatial arrangement.

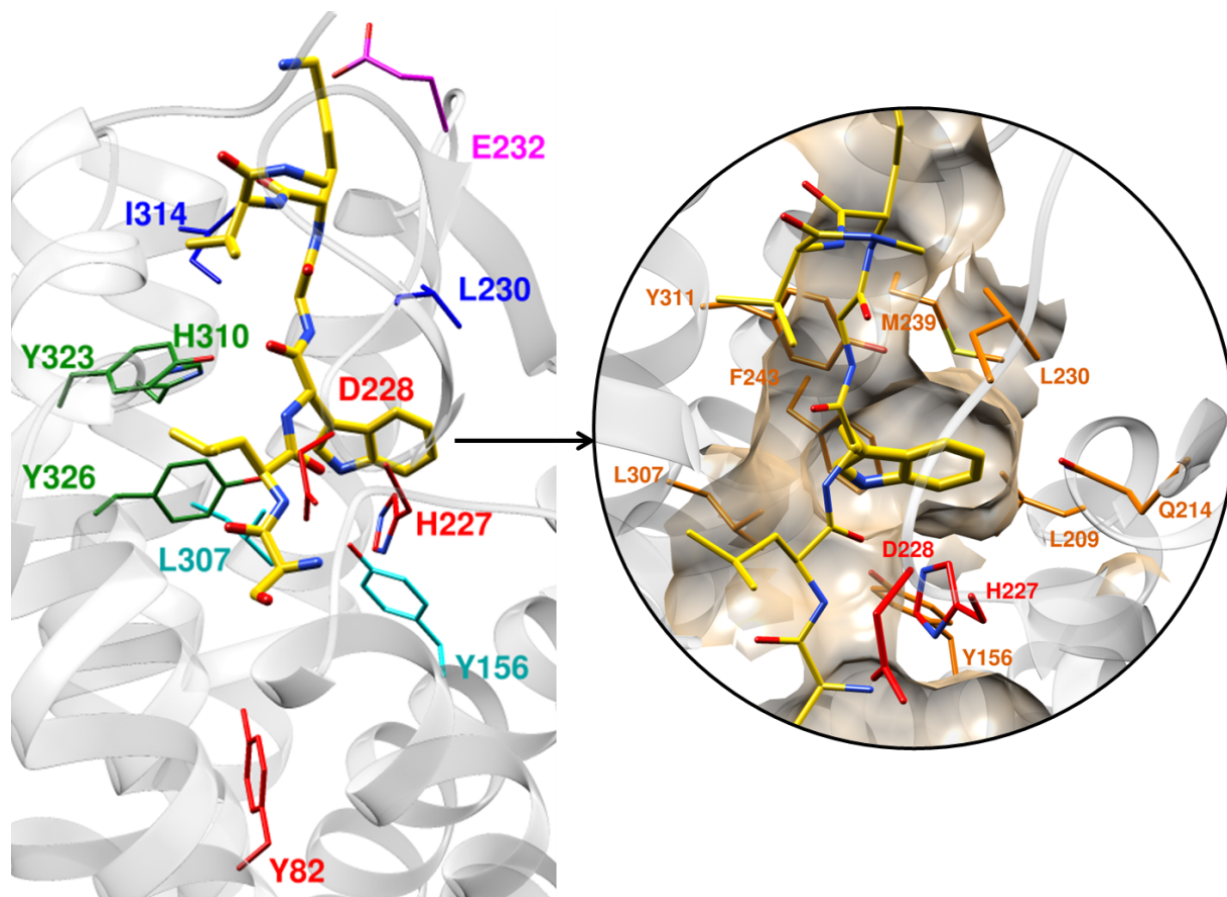


Figure S12. Predicted binding mode of SLWGKV. The ligand and selected residues are shown in sticks. The complex was obtained by molecular docking to the model of agonist-bound PAR2. Receptor residues have been color-coordinated based on their spatial arrangement.

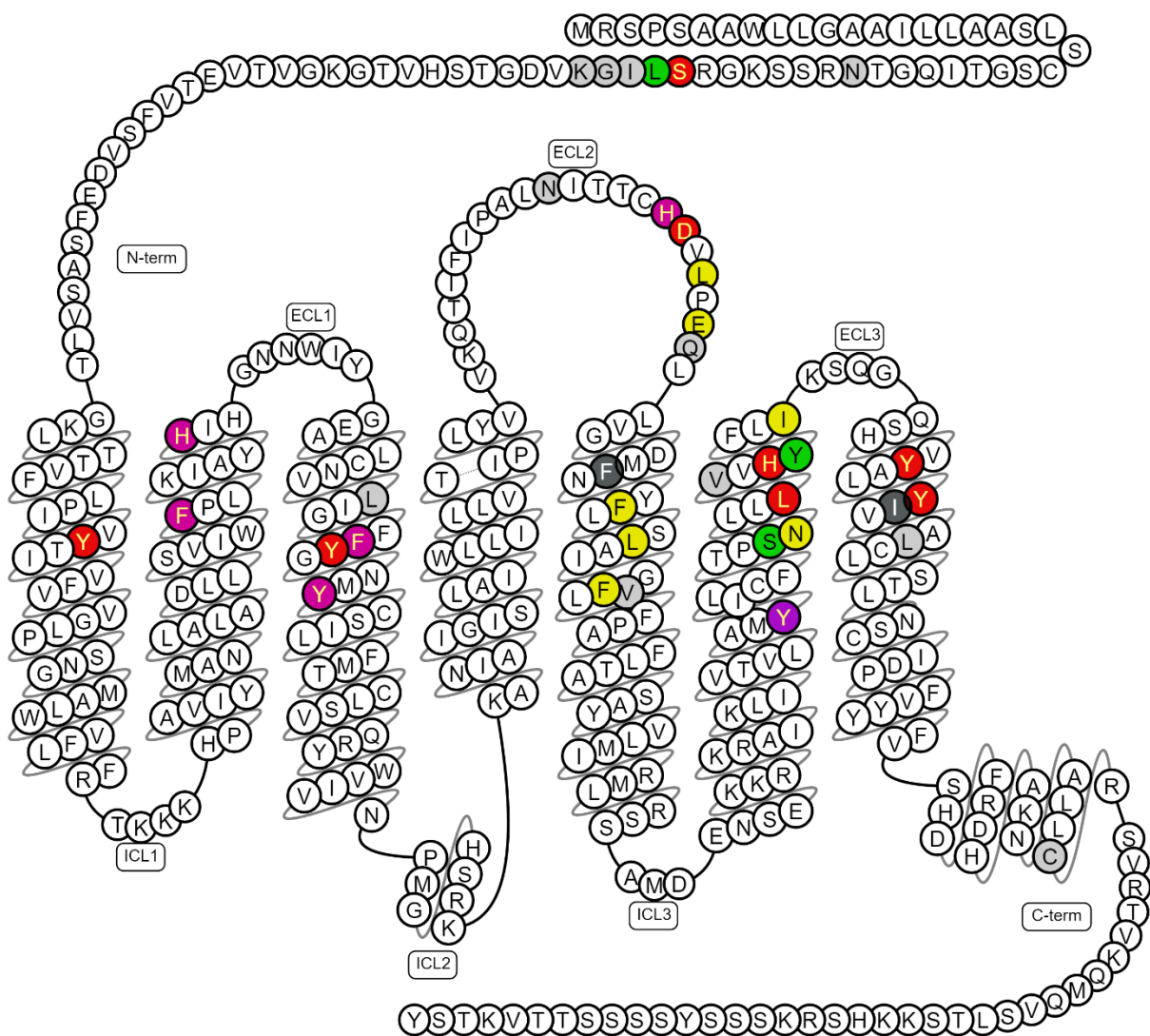


Figure S13. Snake plot generated using the GPCRdb server³ summarizing all point mutations characterized by agonist (trypsin, SLIGKV-NH₂, SLIGRL-NH₂, or 2f-LIGRLO-NH₂) activation from studies outlined in Table S3. Residues have been color-coded based on their fold change effect in calcium mobilization assays (EC_{50} mutant/ EC_{50} WT). For receptor residues mutated to an alanine: ≥ 100 -fold (red); ≥ 50 -fold (purple); ≥ 10 -fold (yellow); ≥ 5 -fold (green) and < 5 -fold (light grey). For receptor residues mutated to a non-alanine mutation: 5–15-fold (magenta); < 5 -fold (dark grey).

TABLES

Table S1. Comparison of affinity and potency data. pK_i was determined in competition binding experiments with [3 H]-GB110 and pEC_{50} in calcium mobilization assays. Data are presented as mean \pm s.e.m of n=2-3 independent experiments.

	$pK_i \pm s.e.m$	$pEC_{50} \pm s.e.m$
SLIGKV	6.32 \pm 0.05	6.06 \pm 0.03
SLIGEV	4.8 \pm 0.2	4.69 \pm 0.06
SLIGAV	4.95 \pm 0.03	5.16 \pm 0.04
SAIGKV	< 3.3	< 3.5
SLAGKV	4.75 \pm 0.06	4.83 \pm 0.03
SL[Chg]GKV	8.1 \pm 0.4	6.58 \pm 0.04
GB110	8.2 \pm 0.3	8.02 \pm 0.09

Table S2. Potency data of endogenous protease trypsin at WT and mutant PAR2 receptors determined in calcium mobilization assays. pEC₅₀ values are shown as mean±s.e.m (n=2-3 independent experiments). Fold change was calculated compared to the response of trypsin at WT PAR2.

	Trypsin	Fold Change
WT	8.24±0.03	1
I321N1	< 6	-
Y323A ^{7.32}	6.57±0.03	48
D228N ^{ECL2}	7.03±0.06	17
Y156A ^{3.33}	7.06±0.04	16
H310A ^{6.58}	7.37±0.04	7
H135Y ^{2.64}	7.6±0.1	5
I314A ^{6.62}	7.60±0.06	4
D228A ^{ECL2}	7.63±0.06	4
H227Q ^{ECL2}	7.67±0.02	4
Y326A ^{7.35}	7.76±0.06	3
E232R ^{ECL2} / N222Q ^{ECL2}	7.81±0.03	3
Y82F ^{1.39}	7.83±0.04	3
Y323F ^{7.32}	7.91±0.08	2
Q233A ^{ECL2} / N222Q ^{ECL2}	7.94±0.04	2
L307A ^{6.55}	7.98±0.04	2
H227A ^{ECL2}	8.09±0.03	1
Y311F ^{6.59}	8.10±0.04	1
L330A ^{7.39}	8.11±0.04	1
I327L ^{7.36}	8.14±0.04	1
E232Q ^{ECL2}	8.24±0.02	1
L230A ^{ECL2}	8.32±0.06	1
Y156F ^{3.33}	8.32±0.05	1
E232A ^{ECL2}	8.36±0.04	1
Y326F ^{7.35}	8.47±0.02	1
Y311A ^{6.59}	8.67±0.06	0.4

Table S3. The effect of point mutations on PAR2 activation of calcium signaling by agonists trypsin or synthetic peptide mimetics (SLIGKV, SLIGRL, and 2f-LIGRLO). This summary includes the findings of this paper as well as those in previous literature. Point mutations are illustrated in a snake plot in Figure S13.

Protein	Residue number	Mutation	Fold change (Activity _{mutant} /Activity _{WT})	Experimental readout	Agonist	Reference
Par2_rat	37 ^{N-term} /38 ^{N-term}	S => A/L =>A	inactive	Ca ²⁺ mobilization	trypsin	Al-Ani et al. 2004, ⁴ Ramachandran et al. 2009 ⁵
Par2_rat	37 ^{N-term} /38 ^{N-term}	S => L/L =>S	inactive	Ca ²⁺ mobilization	trypsin	Al-Ani et al. 2004, ⁴ Ramachandran et al. 2009 ⁵
Par2_rat	38 ^{N-term}	L => A	7	Ca ²⁺ mobilization	trypsin	Al-Ani et al. 2004 ⁴
Par2_human	82 ^{1.39}	Y => A	> 2000	Ca ²⁺ mobilization	2f-LIGRLO-NH ₂	Suen et al. 2017 ⁶
Par2_human	82 ^{1.39}	Y => F	5	Ca ²⁺ mobilization	SLIGKV-NH ₂	Kennedy et al. 2018
Par2_human	128 ^{2.57}	F => L	11	Ca ²⁺ mobilization	2f-LIGRLO-NH ₂	Suen et al. 2017 ⁶
Par2_human	135 ^{2.64}	H => Y	5	Ca ²⁺ mobilization	SLIGKV-NH ₂	Kennedy et al. 2018
Par2_human	155 ^{3.32}	F => L	12	Ca ²⁺ mobilization	2f-LIGRLO-NH ₂	Suen et al. 2017 ⁶
Par2_human	156 ^{3.33}	Y => A	135 (110)	Ca ²⁺ mobilization	SLIGKV-NH ₂	Kennedy et al. 2018, Suen et al 2017 ⁶
Par2_human	156 ^{3.33}	Y => L	16	Ca ²⁺ mobilization	2f-LIGRLO-NH ₂	Suen et al. 2017 ⁶
Par2_human	160 ^{3.37}	Y => L	6	Ca ²⁺ mobilization	2f-LIGRLO-NH ₂	Suen et al. 2017 ⁶
Par2_human	227 ^{ECL2}	H => Q	5	Ca ²⁺ mobilization	SLIGKV-NH ₂	Kennedy et al. 2018
Par2_human	228 ^{ECL2}	D => A	124 (140)	Ca ²⁺ mobilization	SLIGKV-NH ₂	Kennedy et al. 2018, Suen et al. 2017 ⁶
Par2_human	228 ^{ECL2}	D => N	332	Ca ²⁺ mobilization	SLIGKV-NH ₂	Kennedy et al. 2018
Par2_human	230 ^{ECL2}	L => A	17	Ca ²⁺ mobilization	SLIGKV-NH ₂	Kennedy et al. 2018
Par2_human	232 ^{ECL2}	E => A	7 (18)	Ca ²⁺ mobilization	SLIGKV-NH ₂	Kennedy et al. 2018, Suen et al 2017 ⁶
Par2_human	232 ^{ECL2}	E => Q	8	Ca ²⁺ mobilization	SLIGKV-NH ₂	Kennedy et al. 2018
Par2_human	232 ^{ECL2} /222 ^{ECL2}	E => R/N => Q	16	Ca ²⁺ mobilization	SLIGKV-NH ₂	Kennedy et al. 2018
Par2_human	232 ^{ECL2} /233 ^{ECL2}	E => A/Q => A	6	Ca ²⁺ mobilization	2f-LIGRLO-NH ₂	Suen et al. 2017 ⁶
Par2_rat	232 ^{ECL2} /233 ^{ECL2}	E => R/E => R	110	Ca ²⁺ mobilization	SLIGRL-NH ₂	Al-Ani et al. 2002, ⁷ Al-Ani et al. 1999 ⁸
Par2_human	243 ^{5.39}	F => A	11	Ca ²⁺ mobilization	2f-LIGRLO-NH ₂	Suen et al. 2017 ⁶

Par2_human	246 ^{5.42}	L => A	13	Ca ²⁺ mobilization	2f-LIGRLO-NH ₂	Suen et al. 2017 ⁶
Par2_human	251 ^{5.47}	F => A	28	Ca ²⁺ mobilization	2f-LIGRLO-NH ₂	Suen et al. 2017 ⁶
Par2_human	296 ^{6.44}	Y => A	51	Ca ²⁺ mobilization	2f-LIGRLO-NH ₂	Suen et al. 2017 ⁶
Par2_human	303 ^{6.51}	S => A	5	Ca ²⁺ mobilization	2f-LIGRLO-NH ₂	Suen et al. 2017 ⁶
Par2_human	304 ^{6.52}	N => A	29	Ca ²⁺ mobilization	2f-LIGRLO-NH ₂	Suen et al. 2017 ⁶
Par2_human	304 ^{6.52}	N => L	40	Ca ²⁺ mobilization	2f-LIGRLO-NH ₂	Suen et al. 2017 ⁶
Par2_human	307 ^{6.55}	L => A	113 (4)	Ca ²⁺ mobilization	SLIGKV-NH ₂	Kennedy et al. 2018, Suen et al. 2017 ⁶
Par2_human	310 ^{6.58}	H => A	> 342	Ca ²⁺ mobilization	SLIGKV-NH ₂	Kennedy et al. 2018
Par2_human	311 ^{6.59}	Y => A	6 (62)	Ca ²⁺ mobilization	SLIGKV-NH ₂	Kennedy et al. 2018, Suen et al 2017 ⁶
Par2_human	314 ^{6.62}	I => A	23	Ca ²⁺ mobilization	SLIGKV-NH ₂	Kennedy et al. 2018
Par2_human	323 ^{7.32}	Y => A	> 342	Ca ²⁺ mobilization	SLIGKV-NH ₂	Kennedy et al. 2018
Par2_human	323 ^{7.32}	Y => F	50	Ca ²⁺ mobilization	SLIGKV-NH ₂	Kennedy et al. 2018
Par2_human	326 ^{7.35}	Y => A	234 (240)	Ca ²⁺ mobilization	SLIGKV-NH ₂	Kennedy et al. 2018, Suen et al 2017 ⁶
Par2_human	326 ^{7.35}	Y => L	6	Ca ²⁺ mobilization	2f-LIGRLO-NH ₂	Suen et al. 2017 ⁶
Par2_human	326 ^{7.35}	Y => F	6	Ca ²⁺ mobilization	SLIGKV-NH ₂	Kennedy et al. 2018

References

- (1) *GraphPad Prism 7 for Windows*, 7.04; GraphPad Software, Inc: La Jolla, CA, USA, 2017.
- (2) Cheng, R. K. Y., Fiez-Vandal, C., Schlenker, O., Edman, K., Aggeler, B., Brown, D. G., Brown, G. A., Cooke, R. M., Dumelin, C. E., Dore, A. S., Geschwindner, S., Grebner, C., Hermansson, N. O., Jazayeri, A., Johansson, P., Leong, L., Prihandoko, R., Rappas, M., Soutter, H., Snijder, A., Sundstrom, L., Tehan, B., Thornton, P., Troast, D., Wiggin, G., Zhukov, A., Marshall, F. H., and Dekker, N. (2017) Structural insight into allosteric modulation of protease-activated receptor 2. *Nature* 545, 112–115.
- (3) Pándy-Szekeres, G., Munk, C., Tsonkov, T. M., Mordalski, S., Harpsøe, K., Hauser, A. S., Bojarski, A. J., and Gloriam, D. E. (2018) GPCRdb in 2018: adding GPCR structure models and ligands. *Nucleic Acids Res.* 46, D440–D446.
- (4) Al-Ani, B., Hansen, K. K., and Hollenberg, M. D. (2004) Proteinase-Activated Receptor-2: Key Role of Amino-Terminal Dipeptide Residues of the Tethered Ligand for Receptor Activation. *Mol. Pharmacol.* 65, 149–156.
- (5) Ramachandran, R., Mihara, K., Mathur, M., Rochdi, M. D., Bouvier, M., Defea, K., and Hollenberg, M. D. (2009) Agonist-biased signaling via proteinase activated receptor-2: differential activation of calcium and mitogen-activated protein kinase pathways. *Mol. Pharmacol.* 76, 791–801.
- (6) Suen, J. Y., Adams, M. N., Lim, J., Madala, P. K., Xu, W., Cotterell, A. J., He, Y., Yau, M. K., Hooper, J. D., and Fairlie, D. P. (2017) Mapping transmembrane residues of proteinase activated receptor 2 (PAR2) that influence ligand-modulated calcium signaling. *Pharmacol. Res.* 117, 328–342.
- (7) Al-Ani, B., Wijesuriya, S. J., and Hollenberg, M. D. (2002) Proteinase-activated receptor 2: differential activation of the receptor by tethered ligand and soluble peptide analogs. *J. Pharmacol. Exp. Ther.* 302, 1046–1054.
- (8) Al-Ani, B., Saifeddine, M., Kawabata, A., and Hollenberg, M. D. (1999) Proteinase activated receptor 2: role of extracellular loop 2 for ligand-mediated activation. *Br. J. Pharmacol.* 128, 1105–1113.